



# CHORUS

This is the accepted manuscript made available via CHORUS. The article has been published as:

## Examining real-time time-dependent density functional theory nonequilibrium simulations for the calculation of electronic stopping power

Dillon C. Yost, Yi Yao, and Yosuke Kanai

Phys. Rev. B **96**, 115134 — Published 19 September 2017

DOI: [10.1103/PhysRevB.96.115134](https://doi.org/10.1103/PhysRevB.96.115134)

# Examining real-time TDDFT non-equilibrium simulations for the calculation of electronic stopping power

Dillon C. Yost, Yi Yao, and Yosuke Kanai  
Department of Chemistry, University of North Carolina at Chapel Hill

## Abstract

In ion irradiation processes, electronic stopping power describes the energy transfer rate from the irradiating ion to the target material's electrons. Due to the scarcity and significant uncertainties in experimental electronic stopping power data for materials beyond simple solids, there has been growing interest in the use of first-principles theory for calculating electronic stopping power. In recent years, advances in high-performance computing have opened the door to fully first-principles non-equilibrium simulations based on real-time time-dependent density functional theory (RT-TDDFT). While it has been demonstrated that the RT-TDDFT approach is capable of predicting electronic stopping power for a wide range of condensed matter systems, there has yet to be an exhaustive examination of the physical and numerical approximations involved and their effects on the calculated stopping power. We discuss the results of such a study for crystalline silicon with protons as irradiating ions. We examine the influences of key approximations in RT-TDDFT non-equilibrium simulations on the calculated electronic stopping power, including approximations related to basis sets, finite size effects, exchange-correlation approximation, pseudopotentials, and more. Finally, we propose a simple and efficient correction scheme to account for the contribution from core electron excitations to the stopping power, as it was found to be significant for large proton velocities.

## I. INTRODUCTION

When an irradiating ion penetrates condensed matter, the ion transfers its kinetic energy via collisions with the nuclei and electrons in the target material. The stopping power for an ion penetrating a material is the key quantity used to describe this energy transfer [1] Stopping power is defined as the kinetic energy loss per unit distance of projectile ion displacement. For irradiating ions with high kinetic energies ( $> \sim 10$  keV/nucleon), collisions with nuclei in the material are negligible. Instead, the ion's kinetic energy is transferred almost entirely via inelastic collisions to the electrons in the material. This phenomenon is known as electronic stopping, and its associated stopping power is referred to as electronic stopping power.

Electronic stopping power has been the focus of scientific research for decades due to its relevance in technological areas as wide-ranging as nuclear power [4,5], ion beam cancer therapy [7,8], aerospace materials [9,10], 3D ion beam lithography [11], and more. While quantifying electronic stopping power has become increasingly important in technology, experimental studies to determine electronic stopping power remain costly and complicated due to the need for advanced particle accelerators. At the same time, ever since the notion of electronic stopping was conceived, a wide range of analytical and simulation methods have been developed in an attempt to predict electronic stopping power and to provide deeper understanding into the mechanisms involved. Early approximated analytical models based on classical Coulomb scattering [12-14] were followed later by Bethe's quantum-mechanical perturbation approach [15] and Lindhard's calculations within the dielectric formalism based on the free-electron gas [16,17]. The formulae developed by Bethe and Lindhard both fall within the linear response formalism, and these approaches, with refinements and added corrections, remain some of the most widely used methods today. In the last 20 years, first-principles electronic structure theory has become available for calculating the microscopic dielectric response matrix in the context of linear response theory [18]. More recent work in this area has employed time-dependent density functional theory (TDDFT) formalism [19] in calculating the dielectric matrix, going beyond the random phase approximation in this context.

In more recent years, advancements in high-performance computing have opened up the possibility of studying electronic stopping by simulating the non-equilibrium response of electrons using first-principles simulations based on TDDFT. The great potential of this approach was demonstrated in work by Pruneda et al. [20] and Hatcher et al. [21]. Using the real-time propagation approach to TDDFT (RT-TDDFT) simulations [22], in which time-dependent Kohn-Sham equations are integrated in time, the non-equilibrium response of the electronic system to the projectile ion can be simulated. In the last 10

years, various aspects of the RT-TDDFT non-equilibrium simulation approach have advanced, and the approach has become increasingly popular and successful in studying electronic stopping in metals [23-27], semiconductors [6,28,29], and insulators [27,30], for a variety of projectile ions and a variety of condensed matter systems, including liquids [30] and two-dimensional materials [31-34]. At the same time, there have been some indications that various physical and numerical approximations in these RT-TDDFT simulations could influence the calculated electronic stopping power curves. However, accurate experimental measurements of stopping power are rare for most materials, and discrepancies between RT-TDDFT and experimental results are hard to quantify.

Within the framework of linear response theory, where TDDFT (i.e. TD-LDA) was used to obtain the dielectric matrix, recent work by Shukri et al. [6,35] discussed that obtaining a converged result is challenging and requires extrapolation schemes, even for relatively simple materials like silicon. In light of these observations and the recent work by Shukri et al. [6,35], we reexamine the RT-TDDFT approach for calculating the electronic stopping power by considering crystalline silicon with a proton as the projectile ion, for which ample experimental results exist. In this article, we first briefly describe the computational methodology by which electronic stopping power is calculated from RT-TDDFT simulations. We then discuss the effects of a range of numerical and physical approximations on calculating the stopping power, identifying the prominent role of the pseudopotential approximation, which not only removes core electrons in calculations but also modifies the behavior of valence electron wavefunctions near the nuclei. We then describe and demonstrate a computationally feasible correction scheme based on single-atom collision, all-electron, RT-TDDFT simulations.

## II. METHOD

### A. Calculating Electronic Stopping Power from RT-TDDFT

We use the real-time propagation approach of TDDFT (RT-TDDFT) for obtaining electronic stopping power. In all simulations, the time-dependent Kohn-Sham (TDKS) equations are integrated for a system in which a classical, energetic proton with constant velocity travels through the material of interest (diamond cubic silicon), giving rise to a time-dependent external potential acting on the electronic system. A detailed description of the particular RT-TDDFT implementation used in this study can be found in Ref. [23]. The average electronic stopping power can be obtained from the results of an RT-TDDFT simulation in a few different ways in practice. Electronic stopping power is defined as the rate of energy transfer from the projectile ion

to the electronic system per unit distance of projectile travel. Thus, the most intuitive approach to calculate stopping power is to determine the slope of total electronic energy versus time given from the RT-TDDFT simulations. This approach requires a choice of linear regression and/or spline fitting, and it can influence the calculated stopping power, especially for higher projectile ion velocities. Alternatively, it can be shown that the non-adiabatic (NA) force on the projectile is equivalent to the instantaneous electronic stopping power [24]. Thus, for crystalline systems like diamond cubic silicon, we can average the NA force on the projectile over a distance that is an integer multiple of the periodicity of the crystal to precisely calculate the electronic stopping power for a given projectile path and velocity (see Supplemental Material at [URL] for details on the calculation of stopping power from NA force). In this work, we use the latter approach based on the NA force because of its unambiguity for crystalline systems like silicon.

## B. Computational details

We first discuss the observed problem of underestimating the electronic stopping power at high proton velocities via the RT-TDDFT simulations in which the ground-state DFT calculations are sufficiently converged. In our plane-wave-pseudopotential (PW-PP) RT-TDDFT implementation in the Qb@ll/Qbox code [36], the time-dependent Kohn-Sham (TDKS) equations are propagated as the proton penetrates through silicon. We consider the case of the diamond crystalline phase of silicon because there exists a large amount of experimental data. Also, various approximations, such as the semi-local exchange-correlation (XC) potential, in DFT are sufficiently accurate for ground-state properties of silicon. We use the Perdew-Burke-Ernzerhof (PBE) XC functional [37], and we use the adiabatic approximation for its time-dependence [38,39].

Norm-conserving pseudopotentials [40] of the Hamann-Schluter-Chiang-Vanderbilt type [41] were used for all atoms, including the projectile proton. Within this pseudopotential (PP) framework, the 4 valence electrons of each silicon target atom were treated explicitly. The PP cutoff radii of the 3s and 3p electrons of Silicon are 1.1 a.u. and 1.3 a.u., respectively. The PP cutoff radius for the 1s orbital of the Hydrogen projectile atom is 1.0 a.u. We used a large cubic simulation supercell of 216 atoms with the experimental lattice constant of 10.26 Bohr. Prior to performing the RT-TDDFT simulations, the ground state DFT calculation on the crystalline silicon supercell is carried out using the aforementioned computational parameters. It should be noted that no projectile ion is included in this ground-state DFT calculation because the purpose here is to acquire the unperturbed silicon electronic density to be used as the initial condition for the RT-

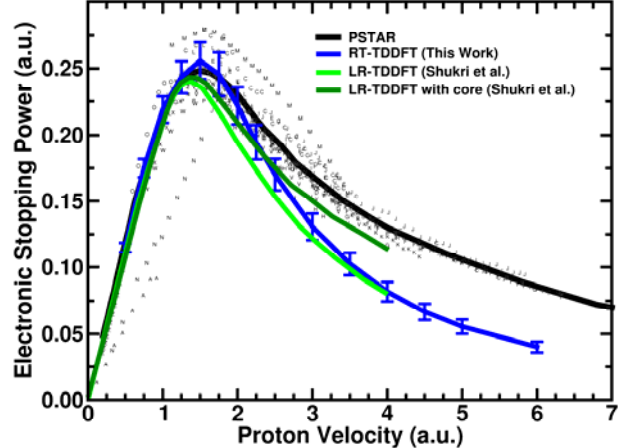


FIG. 1. Electronic stopping power as a function of the velocity of a proton projectile in silicon. The solid black curve represents the empirical PSTAR model [2]. The sets of letters correspond to different experimental data sets that can be found in Ref. [3]. The green curves represent results from the dielectric response formalism using LR-TDDFT for calculating the dielectric matrix [6] with the core electron correction (dark green) and without (light green). The solid blue curve corresponds to the values we obtained by calculating using RT-TDDFT with the “standard” parameters and approximations described in the Methods section. The error bars represent standard deviations of the mean stopping power along the given proton trajectory, which is calculated as an average of the instantaneous force on the projectile proton.

TDDFT simulations. In the RT-TDDFT simulations, the projectile ion, a proton, is treated classically on an equal footing with all of the other ions in the simulation cell, with the exception that it moves at a constant velocity through the simulation cell, all other atoms being held fixed. We used only the gamma point for Brillouin zone sampling. The planewave (PW) cutoff is 50 Ryd.

This “standard” computational procedure is based on parameters that are sufficiently converged at the ground state DFT level for most ground-state properties, including the band gap (0.60 eV). The TDKS equations are integrated using an enforced time reversal symmetry (ETRS) propagator [42], with an integration time step of 0.5 attoseconds. The convergence for the stopping power calculation was confirmed by comparing to a smaller time step of 0.25 attoseconds (see Supplemental Material at [URL] for comparison of stopping power calculated with different time steps).

Instead of converging a classical ensemble average of projectile paths, the so-called “centroid path approximation” for the projectile path as demonstrated for 2D materials in [33] and validated for 3D materials in [28] was used in order to reduce the very large computational

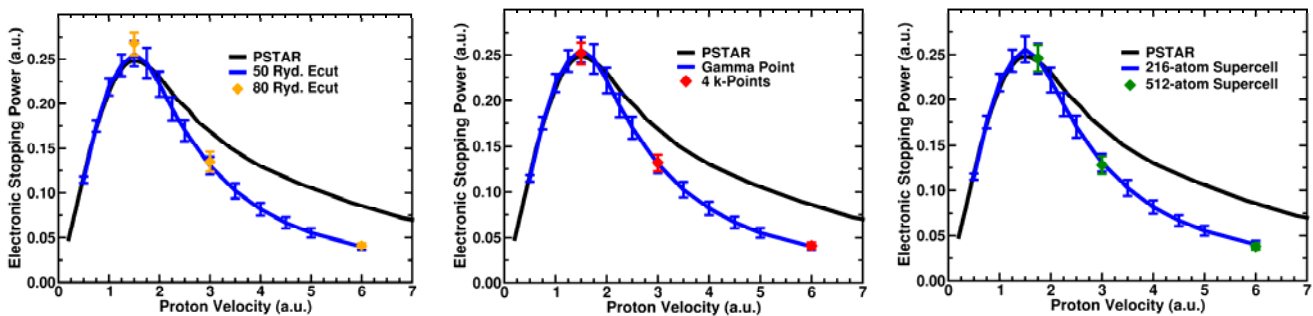


FIG. 2. Electronic stopping power as a function of the velocity of a proton projectile in silicon. The black curve represents the empirically fitted PSTAR model [2]. Convergence of the electronic stopping power curves with respect to various parameters are shown: (left) Calculations with 80 Rydberg planewave kinetic cutoff energy and 50 Rydberg planewave kinetic cutoff energy. (center) Calculations with 4 k-points in the Brillouin zone and only the gamma point in the Brillouin zone. (right) Calculations with at 512-atom supercell and a 216-atom supercell.

cost of RT-TDDFT simulations. As shown in our earlier work for the electronic stopping power of silicon carbide [28], the centroid path approximation does not introduce noticeable errors: The stopping power curves agree well between the stopping power calculations with and without the approximation for the computational framework described above.

In Figure 1, the stopping power results from the RT-TDDFT simulations are shown in comparison to the PSTAR empirical model [2], a wide array of experimentally reported values from the IAEA Nuclear Data Services database [3], and the LR-TDDFT results by Shukri, et al [6]. Exact details of each experimental data set can be found in Ref. [3] and the references therein. This figure and all of the following figures are presented in atomic units. The calculated RT-TDDFT values are in good agreement with the PSTAR model in the velocity regime at and below the Bragg peak ( $v \lesssim 1.5$  a.u.). However, continuing into the high velocity regime, the RT-TDDFT simulation results significantly underestimate the electronic stopping power (52.5% difference at  $v = 6.0$  a.u.) We can be confident that this underestimation does not indicate inaccuracy of the PSTAR model since all reported experimental data agree among them, showing a higher stopping power than our RT-TDDFT result. We note here that this underestimation is not unique to the target material of crystalline silicon, nor is it unique to the proton projectile ion. Previous RT-TDDFT studies indeed have shown similar degrees of disagreement with experiment for electronic stopping power for high-velocity protons and  $\alpha$  particles in water [30], aluminum [24], and silicon carbide [28]. We also note that the relativistic Bethe formula [43] shows that taking the relativistic effect into account changes the stopping power only by +0.005% at  $v = 6.0$  a.u. since the proton velocity is still only a small fraction of the speed of light even at such a large velocity. In Figure 1, we also include the corresponding stopping power curve from

the linear response theory calculations in which the dielectric matrix was obtained from TDDFT [6]. While this result by Shukri et al. also showed the underestimation at high velocities, accounting for the semi-core electrons (2s and 2p electrons of silicon atoms) using an extrapolation scheme largely corrected the underestimation. Motivated by this work using linear response theory, we systematically revisit our non-equilibrium dynamics simulation approach based on RT-TDDFT and examine computational parameters and physical approximations in the following sections.

## IV. RESULTS AND DISCUSSION

### A. Convergence of computational parameters

#### 1. Basis set

In order to examine the influence of the basis set in the plane-wave expansion, we used a higher plane-wave (PW) kinetic energy cutoff of 80 Rydberg, which is much larger than that which is required for converging ground-state properties, including the band structure. Due to the increased computational cost, we examined stopping power for only three velocities:  $v = 6.0$  a.u. (high velocity),  $v = 3.0$  a.u. (mid-range velocity) and  $v = 1.5$  a.u. (near the Bragg peak). As can be seen in Figure 2, the 80 Rydberg simulation result shows no significant difference from the 50 Rydberg simulation (+2.5%) for  $v = 6.0$  a.u. For  $v = 1.5$  a.u., there is a slightly larger difference (+4.5%). The underestimation of electronic stopping power at high velocities cannot be attributed to incompleteness of the basis size.

#### 2. Brillouin zone sampling

Another possible contributor to the stopping power high velocity underestimation problem is insufficient sampling of the Brillouin zone with the single Gamma

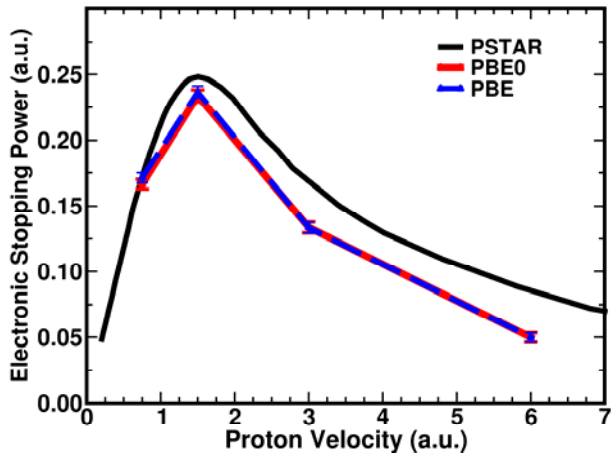


FIG. 3. Electronic stopping power as a function of the velocity of a proton projectile in Si. The solid black curve represents the empirical PSTAR model [2]. The colored curves correspond to the values we obtained by calculating using mixed Gaussian planewave (GPW) RT-TDDFT using the PBE XC functional (dashed blue) and the PBE0 hybrid XC functional (red). The error bars represent standard deviations of the mean stopping power along the given proton trajectory, which is calculated as an average of the instantaneous force on the projectile proton.

point approximation. We performed RT-TDDFT simulations for three proton velocities ( $v = 1.5$  a.u.,  $v = 3.0$  a.u., and  $v = 6.0$  a.u.) using 4 Monkhorst-Pack  $k$ -points. As can be seen in Figure 2, increasing the  $k$ -point sampling in the Brillouin zone has no significant effect on the calculated electronic stopping power values. Considering that a large supercell containing 216 silicon atoms is used, it is not surprising that the gamma point is sufficient to sample the Brillouin zone.

### 3. Finite-size effect

Finite size errors could possibly be responsible for the stopping power underestimation at high velocities. While the convergence of the calculation with respect to the  $k$ -point sampling in the Brillouin zone is not a problem as discussed above, non-physical interactions among periodic images need to be examined in the calculations with the periodic boundary conditions (PBC). Note that a constant shift in the total energy as in the Makov-Payne correction [44] does not change the stopping power values. Figure 2 shows the stopping power using a large 512-atom supercell with 2048 electrons. As can be seen, finite size errors are negligible, and they do not explain the underestimation of our electronic stopping power curve for the high velocity region.

### 4. Exchange-correlation approximation

In the “standard” simulations, we employed the non-empirical generalized gradient approximation (GGA)

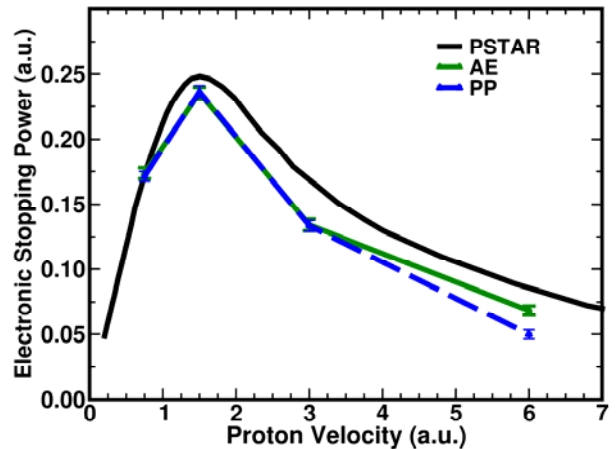


FIG. 4. Electronic stopping power as a function of the velocity of a proton projectile in Si. The solid black curve represents the empirical PSTAR model [2]. The colored curves correspond to the values we obtained by calculating using mixed Gaussian planewave (GPW) RT-TDDFT in which core electrons are treated using pseudopotentials (blue) and treated explicitly using the all-electron approach (green). The error bars represent standard deviations of the mean stopping power along the given proton trajectory, which is calculated as an average of the instantaneous force on the projectile proton.

functional, PBE [37], for our studies because of its balanced accuracy and efficiency, and the GGA XC approximation is particularly convenient for planewave (PW) implementations. At the same time, there exist other more advanced XC approximations such as PBE0 [45]. However, the computational cost of hybrid XC functionals

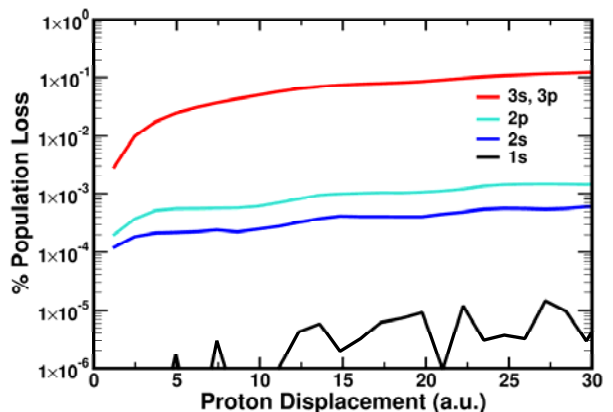


FIG. 5. Population analysis based on projections of the time-dependent Kohn Sham (TDKS) states onto the ground eigenstates of the silicon system. Percentages of population loss relative to the initial, fully occupied condition for the 3s and 3p atomic orbitals (red), the 2p orbitals (light blue), the 2s atomic orbitals (blue), and the 1s atomic orbitals (black) of the silicon atoms.

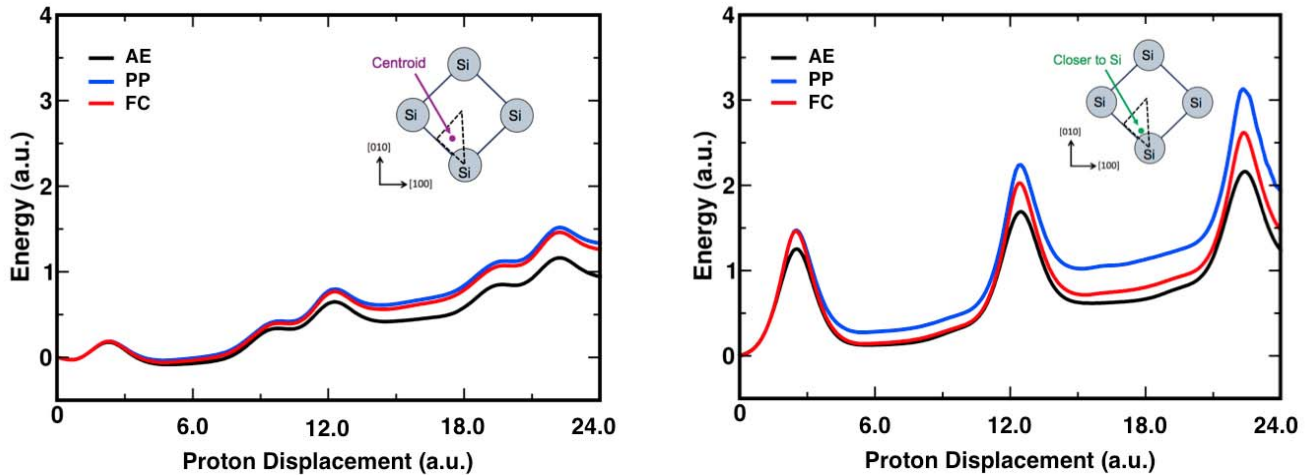


FIG. 6. Total energy as a function of projectile proton ( $v=6.0$  a.u.) displacement in the simulation cell acquired from the RT-TDDFT simulations using the mixed GPW/GAPW approaches. In each plot, the results from three different treatments for the core (1s, 2s, 2p) electrons are shown: The black curve represents the simulation results in which the core electrons are represented by pseudopotentials (PP). The blue curve represents the all-electron (AE) results from using the GAPW method in which the core electrons are treated explicitly and allowed to be excited. The red curve represents the frozen-core (FC) results in which the AE wavefunctions are used but the core electrons are not propagated in time. (left) The results from the simulations for the centroid path trajectory. (right) The results from the simulations for a path parallel to the centroid path trajectory but 33% closer to the channel of target Si atoms.

like PBE0 is prohibitively large in PW-PP implementations because of the calculation of the Hartree-Fock (HF) integral. The majority of approximations/techniques that are used in the PW-PP framework for hybrid XC functionals do not translate well to an RT-TDDFT implementation. For this reason, we used the RT-TDDFT implementation in the CP2K code based on the mixed Gaussian and plane-wave approach (GPW) [46] to examine the influence of the XC approximation. In this approach, KS wavefunctions are represented using Gaussian functions, while the electron density is represented using plane-waves (i.e. GPW/GAPW formalism). We used the ETRS integrator with a time step of 0.5 attoseconds. The DZV3P Gaussian basis set was used for the KS wavefunctions, with Goedecker-Teter-Hutter (GTH) pseudopotentials for core electrons [47]. The electron density is represented in plane-waves with an energy cutoff of 250 Ryd. The HF exchange in PBE0 was computed using the auxiliary density matrix method with the cFIT3 auxiliary basis set [48]. Our test with different basis sets show that DZV3P basis set is sufficiently large for describing the electronic stopping for this material (see Supplemental Material at [URL] for basis set convergence data).

We compare the RT-TDDFT electronic stopping power using the PBE and PBE0 functionals as implemented in the Libxc library [49]. Because of the high computational cost of the PBE0 approximation, we performed simulations only for a few selected proton velocities of interest:  $v=0.5$ , 1.5, 3.0, and 6.0 a.u. Figure 3 shows no significant difference between the PBE and the PBE0 approximations, especially at the high velocities. While the electronic stopping power at these velocities show no significant difference between

the PBE and PBE0 XC functionals, the same may not be true for the threshold velocity at which the stopping power diminishes at low kinetic energies: This is due to the fact that the threshold velocity is directly related to the energy gap of the material [29], which can be quite sensitive to the choice of XC approximation.

## 5. Pseudopotential approximation

Using linear-response TDDFT and the random-phase approximation (RPA) to calculate the dielectric matrix within the framework of Lindhard's linear response model, Shukri, et al. reported the electronic stopping for silicon [6]. The linear response approach is generally considered to be reliable for large velocities. However, Shukri, et al. showed that the stopping power was significantly underestimated at large velocities, similar to our predictions based on RT-TDDFT. In this case of underestimation, however, semi-core electrons were not taken into account when calculating the electronic stopping power (see Figure 1). In the same work, Shukri, et al. proposed an extrapolation scheme to obtain the stopping power curve because converging numerical parameters such as the number of empty bands, number of k-points, and cutoff energy is currently challenging, especially for semi-core electrons (2s and 2p electrons of silicon atoms). Using the extrapolation scheme, and incorporating semi-core electrons, they showed that the electronic stopping power increased by 41% at  $v = 4.0$  a.u. (see Figure 1). They did not consider the contribution to the stopping power from 1s electron in silicon atoms.

Within our "standard" RT-TDDFT simulations in the PW-PP framework, there are two notable deficiencies. One deficiency is that core electrons (i.e. 1s, 2s, and 2p electrons of silicon atoms) are not treated explicitly in the

simulations, and therefore the calculated stopping power does not take into account any electronic excitations from core electrons. Second, using norm-conserving PPs, the wavefunctions for valence electrons do not behave properly within the PP cutoff radius. The total volume taken up by the PP volume amounts only to 5% ( $r_{\text{cut}}=1.1$  a.u.)  $\sim$  7% ( $r_{\text{cut}}=1.3$  a.u.) of the total simulation cell volume, but the excitations from the core electrons likely become more dominant in electronic stopping at large velocities and during close ion-atom collisions. Unfortunately, it is prohibitively computationally expensive to represent all core electrons using plane-waves due to the fact that cutoff energies of hundreds of Rydbergs are required for convergence. Thus, we again used the RT-TDDFT simulations based on the Gaussian and augmented plane-wave method (GAPW) as implemented in the CP2K code for all-electron (AE) calculations to examine this aspect [46,47]. For AE calculations, the 6-311G\*\*3P basis set was used, in which the 6-311G\*\* basis set [50] was combined with 3 additional polarization basis functions taken from the DZV3P basis sets. Our test shows that DZV3P and the 6-311 G\*\*3P basis sets yield the same stopping power (see Supplemental Material at [URL] for basis set convergence data). With the AE simulations, the integration step size needed to be reduced by approximately 50% for numerical stability for the time integration. F

Figure 4 shows the comparison between the all-electron (AE) simulation results and the pseudopotential (PP) simulation results. At the high velocity of  $v = 6.0$  a.u., there is a noticeable difference between the AE and PP simulation results. The stopping power is approximately 30% higher with the AE calculation compared to the PP calculation. In order to analyze the contribution from core electrons to the underlying electronic excitations, we projected the time-dependent Kohn-Sham (TDKS) wavefunctions onto the eigenstates of the system (see Supplemental Material at [URL] for more information on the TDKS projections results). The eigenstates that derived from 1s, 2s, and 2p orbitals of silicon atoms are at  $-1776$  eV,  $-134$  eV,  $-91$  eV below the valence band maximum (VBM), which is mainly composed of the 3s and 3p orbitals of silicon atoms. The projection of the TDKS wavefunctions onto these eigenfunctions shows that the occupations of the valence band (VB) eigenstates decrease due to the electronic excitations that take place in the electronic stopping process, as expected. The time-dependent changes of the occupation for the eigenstates for the 1s, 2s, 2p, and valence electrons at the proton velocity of 6 a.u. are represented in Figure 5. For the 1s state, the occupation decreases only slightly. For the 2s, and 2p states, the decreasing occupations are more substantial. Using the KS eigen-energies and the changes in the occupations, we estimate the extent to which the electronic stopping power is due to the single-particle excitations of these core electrons. The relative contributions of 1s, 2s, and 2p excitations to the stopping power are estimated to be

approximately 0.3%, 1.5%, and 7.9% of the contribution from valence electron excitations. The result clearly shows that the PP approximation can be problematic in simulations of electronic stopping at high velocities. Importantly, this finding also calls for a reexamination of the validity of the centroid path approximation [28,33] for the large velocities because along this path, the proton projectile does not come near the target silicon atoms.

## B. Analysis of core electron effects

In addition to the AE and PP calculations, we also performed AE simulations in which the core electrons are not propagated in time. In these “frozen core (FC)” simulations, core electrons are restricted but the valence-electron wavefunctions correctly behave near the nuclei (except at the cusp). Figure 6 shows the comparison among the all-electron (AE) calculation, the frozen-core (FC) calculation, and the pseudopotential (PP) calculation results. In each of these simulations, we used the centroid path approximation (CPA) in which the closest distance from the projectile proton to a silicon atom is 1.9 a.u. Fig 6 (a) shows that the FC result is much closer to the AE result than to the PP result. Thus, for the CPA trajectory, the difference between the AE and PP calculations does not arise mainly as a result of core electron excitations, but rather it is the valence-electron wavefunction behavior close to the nuclei that is responsible. Fig 6 (b) shows the same set of simulations, but now the proton projectile path is closer to silicon atoms such that the minimum projectile-target distance is  $\sim 1.3$  a.u. (instead of the 1.9 a.u. in the CPA). In this case, the AE-vs-PP difference primarily derives from core electron excitations. The analysis based on the KS eigen-energies shows that the relative contributions of 1s, 2s, and 2p excitations to the stopping power are approximately 0.6%, 6.6%, and 22.9% of the contribution from valence electron excitations, being much larger than the centroid path trajectory. Although the centroid path approximation has been found to be satisfactory for calculating the electronic stopping power of various materials using simulations with pseudopotentials, this approximation becomes less satisfactory when core electron effects are important as shown in the all-electron RT-TDDFT calculations. At high velocities, semi-core electron excitations contribute significantly to the electronic stopping. Unfortunately, converging the stopping power with respect to the ensemble average of proton trajectories in all-electron RT-TDDFT simulations (3024 electrons) comes at a prohibitive computational expense. This is due to two factors: Small regions of the total simulation cell ( $< 10\%$ ) dominate the excitations at high velocities, implying that a large number of random trajectories would be required to converge the ensemble average. Additionally, stable numerical integration of the TD-KS equations becomes highly difficult during close collisions between the projectile ion and target atom nuclei, requiring a very



small discrete time step, and this is also coupled with the fact that very high planewave kinetic cutoff energy is required if the PW-PP formalism is used.

### C. Proposed correction scheme

Here we propose a simple and efficient correction scheme to account for the missing ‘‘core electron’’ effects. We consider obtaining the corrected electronic stopping power  $\bar{S}$  for silicon by scaling the stopping power that is obtained from the RT-TDDFT simulations by a velocity-dependent correction factor  $F_{core}(v)$ , that takes into account the core-electron effects,

$$\bar{S}(v) = S_{CP+PP}(v) \cdot (1 + F_{core}(v)) \quad (1)$$

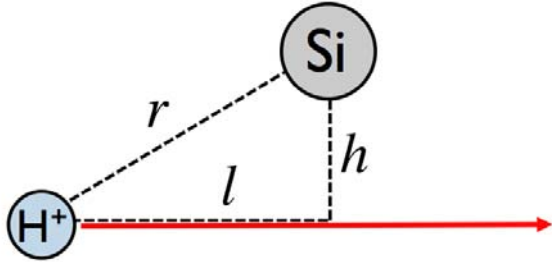


FIG. 7. Scheme for the single-atom collision simulations, where the red arrow indicates the trajectory of the proton ( $H^+$ ). The simulation is carried out over a range of impact parameters  $h$ . The distance between the proton and the Silicon target atom is given by  $r$ . The displacement of the proton is given by  $l$ .

where  $S_{CP+PP}$  is the stopping power acquired in the ‘‘standard’’ simulations using the centroid path approximation and the PP approximation. The scaling factor is given in terms of the ratio between the core and valence electron contributions to the electronic stopping for a *single* silicon atom such that

$$F_{core}(v) = \sum_{i=1}^N \int dV \frac{S_{core}^{Atm}(v, r_i)}{S_{val}^{Atm}(v, r_i)} \quad (2)$$

where the integrand is the ratio between the core and valence electron contributions, which are functions of the distance between the projectile proton and the target silicon atom (in addition to the velocity dependence). The volume integral contains all of the projectile proton position in the simulation cell, and the variable  $r_i$  is the distance to all  $N$  silicon atoms in the simulation cell. In practice, it is not

necessary to consider the atoms that are beyond a small radius ( $\sim 5$  a.u.) of the projectile ion since  $S_{val/core}$  becomes zero at large distances. The distance-dependent  $S_{val/core}$  are related to the total energy transfer that depends on the impact parameter,  $h$ , as (see Figure 8)

$$\int_{-\infty}^{\infty} S_{val/core}^{Atm}(v, r) dl = \Delta E_{val/core}(v, h) \quad (3)$$

We observed from the single-atom RT-TDDFT simulations that, for a given projectile ion velocity, the energy transfer function follow closely a Gaussian function

$$\Delta E_{val/core}(v, h) = A_{val/core}(v) e^{-B_{val/core}(v)h^2} \quad (4)$$

By expressing  $\Delta E_{val/core}$  also as

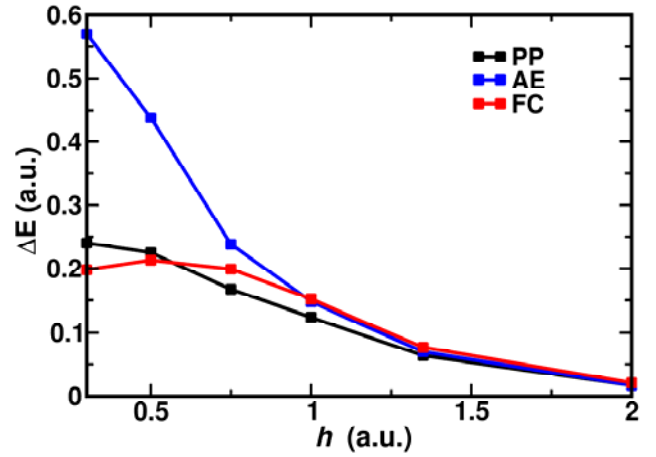


FIG. 8. Energy transferred in single-atom collision simulations as a function of impact parameter  $h$  for the simulations using pseudopotentials (black), all electrons (blue), and frozen core (red) schemes. See the text for details.

$$S_{val/core}^{Atm}(v, r) = C_{val/core}(v) e^{D_{val/core}(v)r^2} \quad (5)$$

for numerical convenience. Geometric relationships between  $r$ ,  $h$ , and  $l$  of Figure 7 then yield

$$D(v) = B(v) \quad (6)$$

and

$$C(v) = A(v) \sqrt{\frac{B(v)}{\pi}} \quad (7)$$

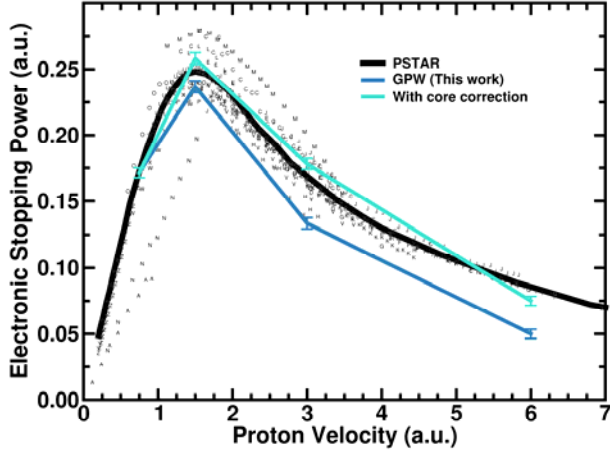


FIG. 9. Electronic stopping power as a function of the velocity of a proton projectile in Si. The solid black curve represents the empirical PSTAR model [2]. The sets of letters correspond to different experimental data sets that can be found in Ref. [3]. The dark blue curve corresponds to the values we obtained by calculating using mixed Gaussian planewave (GPW) RT-TDDFT with the “standard” parameters and approximations described in the Methods section. The light blue curve corresponds to the results after the core correction has been applied. The error bars represent standard deviations of the mean stopping power for the trajectory.

We can thus determine these coefficients  $D(v)$  and  $C(v)$  via Eq. 6 and Eq. 7 by finding the parameters  $A$  and  $B$  in Eq. 4 by obtaining  $\Delta E_{val/core}$  from “single-atom simulations” in which the impact parameter between the projectile proton and a single target silicon atom is varied.  $\Delta E_{core}$  is obtained from the AE RT-TDDFT and with the PP approximation as

$$\Delta E_{core}(v, h) = \Delta E_{AE}(v, h) - \Delta E_{val}(v, h). \quad (8)$$

Figure 8 shows the energy transferred versus impact parameter for the single collision simulations for  $v=6.0$  a.u. For impact parameters below  $\sim 0.75$  a.u., the all-electron simulations show significantly higher energy transfer than the PP simulations. The results are fit to the Gaussian function (Eq. 4) to determine the parameters  $A$  and  $B$ . Having determined the shape of  $S_{val/core}^{Atm}$  functions, the velocity-dependent scaling factor is determined to correct for the missing core effects as in Eq. 2.

This correction scheme can be also applied using PW simulations using semi-core PPs, in addition to the all-electron simulations with the GAPW approach. In the semicore PPs, only the 1s electrons are pseudized, and the 2s, 2p, 3s, and 3p electrons of silicon atoms are treated

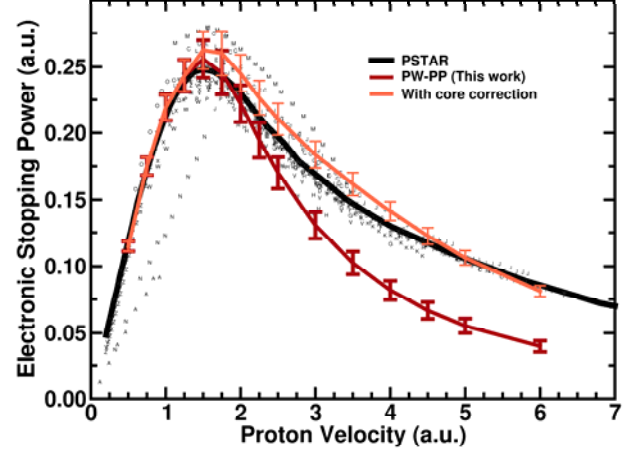


FIG. 10. Electronic stopping power as a function of the velocity of a proton projectile in Si. The solid black curve represents the empirical PSTAR model [2]. The sets of letters correspond to different experimental data sets that can be found in Ref. [3]. The dark red curve corresponds to the values we obtained by calculating using planewave pseudopotential (PW-PP) RT-TDDFT with the “standard” parameters and approximations described in the Methods section. The light red curve corresponds to the results after the core correction has been applied. The error bars represent standard deviations of the mean stopping power for the trajectory.

explicitly. In the expressions given above, the energy transfers in the semi-core PP simulations are used in place of the all-electron single-atom energy transfers. This alternative approach is possible due to the fact that 1s electron excitations contribute less than 1% to the total electronic stopping power. For these single-atom collision simulations, we generated semicore pseudopotentials for Silicon with cutoff radii of 0.40, 0.35, and 0.40 Bohr for the 2s, 2p, and 3p orbitals, respectively, in keeping with the parameters used by Tiago et al. [51]. Due to the very small cutoff radii, a very large planewave cutoff energy of 400 Rydberg was required to converge the energy gap. While this high cutoff energy would make RT-TDDFT simulations with the Silicon supercell prohibitively expensive, the computational cost is manageable for the single-atom collision simulations.

Figure 9 and Figure 10 show the results of applying the core correction factors for the GPW-based (corrected with all-electron single-atom calculations) simulation result and PW-based simulation result (corrected with semi-core PP single-atom calculations), respectively. When these corrections are applied, we observe significant improvement with respect to the experimental data. The corrected GPW and PW electronic stopping power curves show the average absolute % difference relative to the

PSTAR results of 5.1% and 5.2%, respectively. Applying the core correction increases the stopping power by 55% (105%) at  $v = 6.0$  a.u. for the GPW (PW) simulations. For  $v \leq 1.0$  a.u., there is negligible difference between the corrected and uncorrected results. At the Bragg peak ( $v = 2.0$  a.u.), the core correction increases the GPW (PW) electronic stopping power by 9.0% (7.1%).

## V. CONCLUSIONS

We presented a thorough, methodical examination of non-equilibrium electron dynamics simulations based on RT-TDDFT for the calculation of electronic stopping power. We have shown that converging several computational factors, such as k-point sampling, planewave cutoff energy, and exchange-correlation (XC) approximation, with respect to the ground state DFT calculations is sufficient to ensure convergence of RT-TDDFT results. However, we have also identified several approximations that require special attention in these types of simulations. The combination of the centroid path approximation and the pseudopotential approximation leads to a neglect of core electronic effects, which are particularly important at high projectile ion velocities. We showed that core electrons affect electronic stopping in two ways: core electron excitations and modification of the valence wavefunctions near the core regions. We demonstrated that both of these effects contribute to an increase in electronic stopping and that the relative importance of these effects has a strong impact-parameter dependence. Unfortunately, performing RT-TDDFT simulations with all-electrons or semi-core-PPs setup for a classical ensemble of projectile ion trajectories is not yet practical due to the computational expense. As an alternative approach, we proposed a single-atom correction scheme to approximately take into account the missing core electronic excitations for the electronic stopping power calculation.

Another approximation in this work is the adiabatic approximation to the XC potential in RT-TDDFT. This approximation results in having the XC potential that depends only on the instantaneous electron density, neglecting any memory effects [52]. Nazarov *et al.* [53] have shown, within the linear response formalism, that error resulting from the adiabatic approximation is negligible for low-Z ions such as protons and  $\alpha$  particles stopping in a homogeneous electron gas. However, for high-Z ions, the error can be significant. The influence of the adiabatic XC approximation in the RT-TDDFT approach on electronic stopping power needs to be investigated in the future. In the RT-TDDFT approach, having the energy functional as a constant of motion is essential for directly obtaining the electronic stopping power from the electronic energy [23,31], and the stopping power can be calculated equivalently from the Hellman-Feynman force on the projectile ion, as we have done here,

when the adiabatic approximation is used. However, the XC functional, in principle, depends on the electron density at previous times and on the initial wavefunction. As discussed by Ullrich in the context of the current TDDFT [54], deriving an accurate XC approximation that ensures a constant total energy is quite complicated when the adiabatic XC approximation is alleviated. If this were accomplished, one could then also derive the corresponding expression for forces from the resulting action [55], which is unlikely to be the Hellman-Feynman force when the adiabatic XC approximation is not adapted. Going beyond the adiabatic approximation in RT-TDDFT for simulation of real materials is presently out of reach and remains an active area of current research [56,57].

## ACKNOWLEDGMENTS

We acknowledge computational resources from the Argonne Leadership Computing Facility, which is a Department of Energy (DOE) Office of Science User Facility supported under Contract No. DE-AC02-06CH11357. An award of computer time was provided by the Innovative and Novel Computational Impact on Theory and Experiment (INCITE) program. This work is supported by the National Science Foundation under Grants No. CHE-1565714 and No. DGE-1144081.

- [1] C. Race, D. Mason, M. Foo, W. Foulkes, A. Horsfield, and A. Sutton, *Journal of Physics: Condensed Matter* **25**, 125501 (2013).
- [2] M. Berger, J. Coursey, M. Zucker, and J. Chang, (National Institute of Standards and Technology, Gaithersburg, MD, 2005).
- [3] H. Paul and C. Montanari, (International Atomic Energy Agency - Nuclear Data Section, Vienna, Austria, 2007).
- [4] G. R. Odette and B. D. Wirth, in *Handbook of materials Modeling* (Springer, 2005), pp. 999.
- [5] G. S. Was, *Fundamentals of radiation materials science: metals and alloys* (Springer, 2016).
- [6] A. A. Shukri, F. Bruneval, and L. Reining, *Physical Review B* **93**, 035128 (2016).
- [7] O. Obolensky, E. Surdutovich, I. Pshenichnov, I. Mishustin, A. Solov'Yov, and W. Greiner, *Nuclear Instruments and Methods in Physics Research Section B: Beam Interactions with Materials and Atoms* **266**, 1623 (2008).
- [8] A. C. Begg, F. A. Stewart, and C. Vens, *Nature Reviews Cancer* **11**, 239 (2011).
- [9] H. Zeller, *Microelectronics reliability* **37**, 1711 (1997).
- [10] S. Duzellier, *Aerospace science and technology* **9**, 93 (2005).
- [11] H. Kraus *et al.*, *Nano Letters* (2017).

- [12] E. Rutherford, The London, Edinburgh, and Dublin Philosophical Magazine and Journal of Science **21**, 669 (1911).
- [13] J. J. Thomson, The London, Edinburgh, and Dublin Philosophical Magazine and Journal of Science **23**, 449 (1912).
- [14] C. G. Darwin, The London, Edinburgh, and Dublin Philosophical Magazine and Journal of Science **23**, 901 (1912).
- [15] H. Bethe, Annalen der Physik **397**, 325 (1930).
- [16] J. Lindhard, M. Scharff, and H. E. Schiøtt, *Range concepts and heavy ion ranges* (Munksgaard, 1963).
- [17] J. Lindhard and A. Winther, *Stopping power of electron gas and equipartition rule* (Munksgaard, 1964).
- [18] R. J. Mathar, J. R. Sabin, and S. Trickey, Nuclear Instruments and Methods in Physics Research Section B: Beam Interactions with Materials and Atoms **155**, 249 (1999).
- [19] E. Runge and E. K. Gross, Physical Review Letters **52**, 997 (1984).
- [20] J. Pruneda, D. Sánchez-Portal, A. Arnau, J. Juaristi, and E. Artacho, Physical review letters **99**, 235501 (2007).
- [21] R. Hatcher, M. Beck, A. Tackett, and S. T. Pantelides, Physical review letters **100**, 103201 (2008).
- [22] K. Yabana and G. Bertsch, Physical Review B **54**, 4484 (1996).
- [23] A. Schleife, E. W. Draeger, Y. Kanai, and A. A. Correa, The Journal of chemical physics **137**, 22A546 (2012).
- [24] A. Schleife, Y. Kanai, and A. A. Correa, Physical Review B **91**, 014306 (2015).
- [25] E. E. Quashie, B. C. Saha, and A. A. Correa, Physical Review B **94**, 155403 (2016).
- [26] M. A. Zeb, J. Kohanoff, D. Sánchez-Portal, A. Arnau, J. Juaristi, and E. Artacho, Physical review letters **108**, 225504 (2012).
- [27] M. A. Zeb, J. Kohanoff, D. Sánchez-Portal, and E. Artacho, Nuclear Instruments and Methods in Physics Research Section B: Beam Interactions with Materials and Atoms **303**, 59 (2013).
- [28] D. C. Yost and Y. Kanai, Physical Review B **94**, 115107 (2016).
- [29] R. Ullah, F. Corsetti, D. Sánchez-Portal, and E. Artacho, Physical Review B **91**, 125203 (2015).
- [30] K. G. Reeves, Y. Yao, and Y. Kanai, Physical Review B **94**, 041108 (2016).
- [31] Y. Miyamoto and H. Zhang, Physical Review B **77**, 161402 (2008).
- [32] S. Bubin, B. Wang, S. Pantelides, and K. Varga, Physical Review B **85**, 235435 (2012).
- [33] S. Zhao, W. Kang, J. Xue, X. Zhang, and P. Zhang, Journal of Physics: Condensed Matter **27**, 025401 (2014).
- [34] A. Ojanperä, A. V. Krasheninnikov, and M. Puska, Physical Review B **89**, 035120 (2014).
- [35] A. Shukri, Ecole Polytechnique, 2015.
- [36] E. W. Draeger and F. Gygi, Lawrence Livermore National Laboratory Tech. Report. (2014).
- [37] J. P. Perdew, K. Burke, and M. Ernzerhof, Physical review letters **77**, 3865 (1996).
- [38] A. Zangwill and P. Soven, Physical Review Letters **45**, 204 (1980).
- [39] A. Zangwill and P. Soven, Physical Review B **24**, 4121 (1981).
- [40] M. Fuchs and M. Scheffler, Computer Physics Communications **119**, 67 (1999).
- [41] D. Vanderbilt, Physical Review B **32**, 8412 (1985).
- [42] A. Castro, M. A. Marques, J. A. Alonso, G. F. Bertsch, and A. Rubio, The European Physical Journal D-Atomic, Molecular, Optical and Plasma Physics **28**, 211 (2004).
- [43] H. Bethe, Zeitschrift für Physik **76**, 293 (1932).
- [44] G. Makov and M. Payne, Physical Review B **51**, 4014 (1995).
- [45] C. Adamo and V. Barone, The Journal of chemical physics **110**, 6158 (1999).
- [46] J. Hutter, M. Iannuzzi, F. Schiffmann, and J. VandeVondele, Wiley Interdisciplinary Reviews: Computational Molecular Science **4**, 15 (2014).
- [47] S. Goedecker, M. Teter, and J. Hutter, Physical Review B **54**, 1703 (1996).
- [48] M. Guidon, J. Hutter, and J. VandeVondele, Journal of Chemical Theory and Computation **6**, 2348 (2010).
- [49] M. A. Marques, M. J. Oliveira, and T. Burnus, Computer Physics Communications **183**, 2272 (2012).
- [50] The Journal of Chemical Physics **72**, 650 (1980).
- [51] M. L. Tiago, S. Ismail-Beigi, and S. G. Louie, Physical Review B **69**, 125212 (2004).
- [52] C. A. Ullrich, *Time-dependent density-functional theory: concepts and applications* (OUP Oxford, 2011).
- [53] V. Nazarov, J. Pitarke, Y. Takada, G. Vignale, and Y.-C. Chang, Physical Review B **76**, 205103 (2007).
- [54] C. A. Ullrich, The Journal of chemical physics **125**, 234108 (2006).
- [55] T. Kunert and R. Schmidt, The European Physical Journal D-Atomic, Molecular, Optical and Plasma Physics **25**, 15 (2003).
- [56] M. Thiele, E. Gross, and S. Kümmel, Physical review letters **100**, 153004 (2008).
- [57] N. T. Maitra, The Journal of Chemical Physics **144**, 220901 (2016).
- [58] See Supplemental Material at [URL] for information on effective charge analysis of the projectile ion and an accelerated Voronoi analysis scheme, which includes Refs. [59-61].
- [59] G. Henkelman, A. Arnaldsson, and H. Jónsson, Computational Materials Science **36**, 354 (2006).
- [60] W. Tang, E. Sanville, and G. Henkelman, Journal of Physics: Condensed Matter **21**, 084204 (2009).

[61] M. B. Kennel, arXiv preprint physics/0408067 (2004).